ACES Asian Chemical Editorial Society

DOI: 10.1002/ajoc.202000165

ASIAN JOURNAL OF ORGANIC CHEMISTRY Communication

Special Issue

Highly Fluorescent Emitters Based on Triphenylamine-π-Triazine (D-π-A) System: Effect of Extended Conjugation on Singlet-Triplet Energy Gap

Shiv Kumar,[a] Pachaiyappan Rajamalli,[a, b] David B. Cordes,[a] Alexandra M. Z. Slawin,[a] and Eli Zysman-Colman*[a]

Abstract: Three D-π-A type linearly-extended emitters, based on diphenylamine (**DPA**) as the donor and 2,4,6-triphenyl-1,3,5-triazine (**TRZ**) as the acceptor, were synthesized and their optoelectronic properties characterized. The introduction of an additional phenyl or phenylethynyl π-spacer results in an enhancement of the molar extinction coefficient and a systematic bathochromic shift of the charge-transfer transition in the absorption spectra. A mirrored bathochromic shift in the photoluminescence spectra is also observed with increasing conjugation of the bridge moiety. All three compounds show high photoluminescence quantum yields and moderate singlet-triplet excited state energy gaps, ΔE_{ST}, of 0.26-0.37 eV were observed in 10 wt% doped films in mCP as the host matrix.

Introduction

Thermally activated delayed fluorescence (TADF) emitters have become very popular alternatives to phosphorescent organometallic complexes for organic light-emitting diodes (OLEDs) because this class of materials can likewise recruit both singlet (25%) and triplet (75%) excitons to produce light.[1–2] TADF compounds accomplish this through thermal upconversion of triplet excitons into singlet excitons, a process made possible due to the small singlet-triplet excited state energy gap, ΔE_{ST}.[3–4] In order to minimise ΔE_{ST}, the exchange interaction integral, which scales with the spatial overlap between the HOMO and LUMO, must also be minimized.[5] Achieving a highly twisted conformation between donor and acceptor moieties is the most commonly adopted strategy to spatially separate the frontier molecular orbitals in TADF emitters.[6–7]

The 2,4,6-triphenyl-1,3,5-triazine (TRZ) is one the most commonly used acceptor moieties for TADF emitters. The TRZ moiety was first introduced in 2011 by Adachi *et al.*[8] The **PIC-TRZ** (λ_{PL} = 500 nm, ΔE_{ST} = 0.11 eV, Φ_{PL} = 39% in 6 wt% mCP film) was the very first purely organic TADF compound to exhibit bluish-green emission. An OLED device employing this emitter produced a EQE_{max} of 5.1% with emission at λ_{EL} = 500 nm. Subsequently, many highly efficient TADF emitters using TRZ as the acceptor have been developed. A selection of the state-of-the-art emitters based on the TRZ acceptor is shown in Figure 1. In each example, the emitter adopts a highly twisted conformation between donor and acceptor groups. Introduction of methyl groups on the bridging phenyl spacer in deep blue emitters **Cz-Trz 1** (λ_{PL}: 435 nm, ΔE_{ST}: 0.17 eV, Φ_{PL}: 92% in 6 wt% DPEPO film) and **Cz-Trz 2** (λ_{PL}: 432 nm, ΔE_{ST}: 0.15 eV, Φ_{PL}: 85% in 6 wt% DPEPO film) induced a large torsions between the carbazole donor and the TRZ acceptor. OLEDs using these emitters exhibited emission at 450 nm and 452 nm with maximum external quantum efficiencies, EQE_{max} of 19.2 and 18.3% with CIE coordinates of (0.140, 0.098) and (0.150, 0.097), respectively.[9] Replacing carbazole with stronger donors such as phenoxazine (PXZ) or phenothiazine (PTZ) led to green TADF emitters **PXZ-TRZ** (λ_{PL}: 545 nm, ΔE_{ST}: 0.07 eV, Φ_{PL}: 65% in 6 wt% CBP film, EQE_{max}: 12.0% ; λ_{EL}: 545 nm) and **PTZ-TRZ** (λ_{PL}: 540 nm, ΔE_{ST}: 0.07 eV, Φ_{PL}: 65% in 6 wt% CBP film; EQE_{max}: 12.5%; λ_{EL}: 529 nm), respectively.[10–11] The OLED with in **DMAC-TRZ** as the emitter, containing 9,9-dimethylacridan (DMAC) as the donor (λ_{PL} = 495 nm, ΔE_{ST} = 0.04 eV, Φ_{PL} = 90% in 8 wt% mCP film), exhibited an excellent EQE_{max} of 26.5% (λ_{EL} = 500 nm).[12] Adachi *et al.* reported an acceptor-donor-acceptor TADF emitter **DHPZ-2TRZ** (λ_{PL}: 598 nm, ΔE_{ST}: 0.07 eV, Φ_{PL}: 6.6% in 6 wt% mCBP film) incorporating the very strongly electron-donating dihydrophenazine as the donor group. The OLED employing this compound showed red emission at λ_{EL} of 617 nm but with an EQE_{max} of 1%, a result of the very low Φ_{PL} in the doped film.[13] Changing the donor to 4,4′-bis(diphenylamino)phenylamine in **DDPA-TRZ** (λ_{PL}: 540 nm, ΔE_{ST}: 0.11 eV) led to a TADF emitter with Φ_{PL} of unity in 6 wt% mCBP film. Realizing such a high Φ_{PL} in this particular compound was due to a combination of high

[a] Dr. S. Kumar, Prof. P. Rajamalli, Dr. D. B. Cordes, Prof. A. M. Z. Slawin, Prof. E. Zysman-Colman
Organic Semiconductor Centre
EaStCHEM School of Chemistry
University of St Andrews
St Andrews, Fife, KY16 9ST (United Kingdom)
E-mail: eli.zysman-colman@st-andrews.ac.uk
Homepage: http://www.zysman-colman.com

[b] Prof. P. Rajamalli
Current address: Materials Research Centre
Indian Institute of Science
Bangalore 560012 (India)

Supporting information for this article is available on the WWW under https://doi.org/10.1002/ajoc.202000165. The research data supporting this publication can be accessed at https://doi.org/10.17630/1e5be2cf-e463-4d0c-972d-a963c7c404f4

Special Issue *This manuscript is part of a special issue on Organic Donor–Acceptor Systems. A link to the Table of Contents of the special issue will appear here when the complete issue is published.*

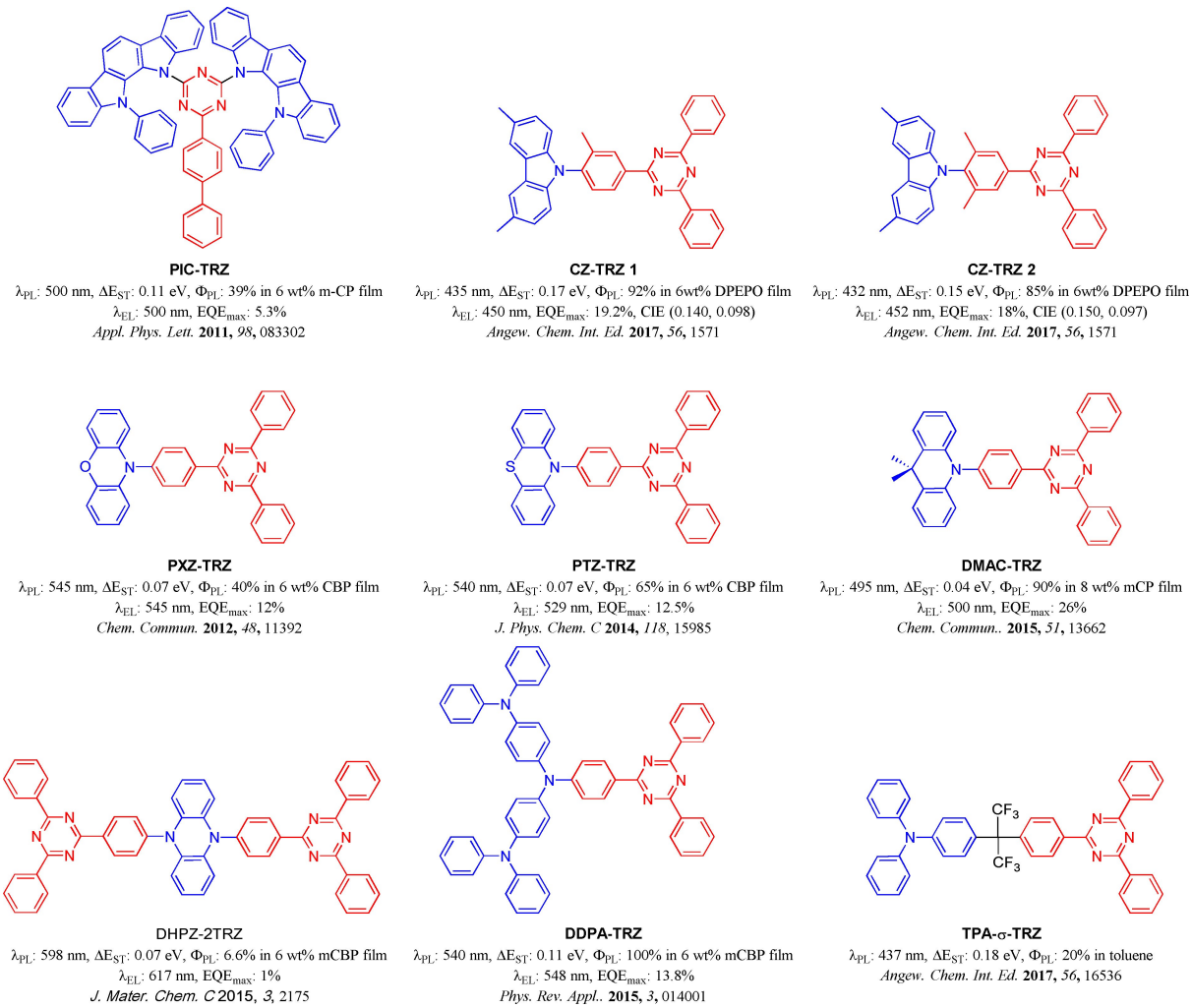

Figure 1. Chemical structures and performance of some of the known triazine-based TADF emitters.

oscillator strength due to the relatively large overlap of the electron density of the HOMO and LUMO and the efficient suppression of non-radiative decay pathways.[14] In 2017, Adachi *et al.* reported a series of TADF emitters containing an sp^3-carbon spacer that effectively breaks conjugation between the donor and acceptor, and emission thus results from intermolecular charge transfer states, analogously to what is observed in exciplexes.[15] The emitters, **DMAC-σ-TRZ** (λ_{PL} = 463 nm, ΔE_{ST} = 0.06 eV, Φ_{PL} = 70% in toluene) and **TMCz-σ-TRZ** (λ_{PL} = 450 nm, ΔE_{ST} = 0.07 eV, Φ_{PL} = 36% in toluene) exhibited remarkably high Φ_{PL} while **TPA-σ-TRZ** (λ_{PL} = 437 nm, ΔE_{ST} = 0.18 eV, Φ_{PL} = 20% in toluene) showed a relatively lower Φ_{PL} that was ascribed to the greater conformational flexibility in this molecule.[15] All of these TRZ-containing examples reveal the importance of the design of the bridging unit to electronically decouple the donor and acceptor groups. However, we have not come across any report in the literature that has explored increasing conjugation length of the bridge to spatially separate the donor and acceptor groups as a strategy to promote electronic decoupling between the two. In the present report, we explore the effect of increasing the conjugation length of the bridge, thereby increasing spacing of the donor and acceptor, on the optoelectronic properties of the emitter.

Herein, we investigated the optoelectronic properties of three triazine-containing emitters, **DPA-TRZ**,[15] **TPA-TRZ** and **TPA-E-TRZ**[16] (Figure 2) and correlated these with the structure of three different bridging units. In particular, this study showcases the balance between the spatial separation of donor and acceptor and the magnitude of the conjugation within the bridging moiety and the effect this has on the relative singlet and triplet excited state energies of the compounds. Both **DPA-TRZ** and **TPA-E-TRZ** are known in the literature. However, only the photophysical properties of **DPA-TRZ** have been reported, and only in a rudimentary fashion, showing a partial absorption spectrum in toluene, a steady-state fluorescence spectrum at 298 K in toluene and a phosphorescence spectrum at 77 K in a toluene glass matrix, the data of which qualitatively match with the photophysics presented in the present study.[15]

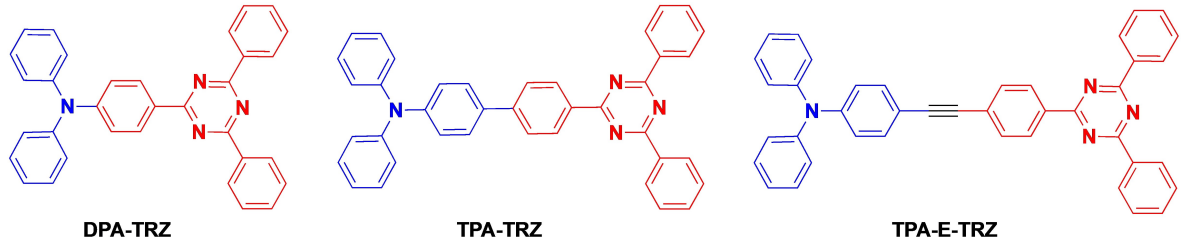

Figure 2. Chemical structure of DPA-TRZ, TPA-TRZ, and TPA-E-TRZ.

Results and Discussion

Synthesis

The three emitters were prepared as outlined in Scheme 1. Both 4-(4,6-diphenyl-1,3,5-triazin-2-yl)-*N*,*N*-diphenylaniline (**DPA-TRZ**)[15] and 4′-(4,6-diphenyl-1,3,5-triazin-2-yl)-*N*,*N*-diphenyl-(1,1′-biphenyl)-4-amine (**TPA-TRZ**) were obtained in modest yield via palladium-catalysed Suzuki-Miyaura cross-coupling of (4-(diphenylamino)phenyl)boronic (**1**) acid with 2-chloro-4,6-diphenyl-1,3,5-triazine (**2**) and 2-(4-bromophenyl)-4,6-diphenyl-1,3,5-triazine (**3**), respectively, while 4-((4-(4,6-diphenyl-1,3,5-triazin-2-yl)phenyl)ethynyl)-*N*,*N*-diphenylaniline (**TPA-E-TRZ**)[16] was prepared in modest yield by Sonogashira cross-coupling reaction between 2-(4-ethynylphenyl)-4,6-diphenyl-1,3,5-triazine (**4**) and 4-bromo-*N*,*N*-diphenylaniline (**5**). The identity of the three compounds was determined by ^{1}H and ^{13}C NMR spectroscopy and high-resolution mass spectrometry (HRMS). Purity of each emitter was established by HPLC, melting point determination and elemental analysis.

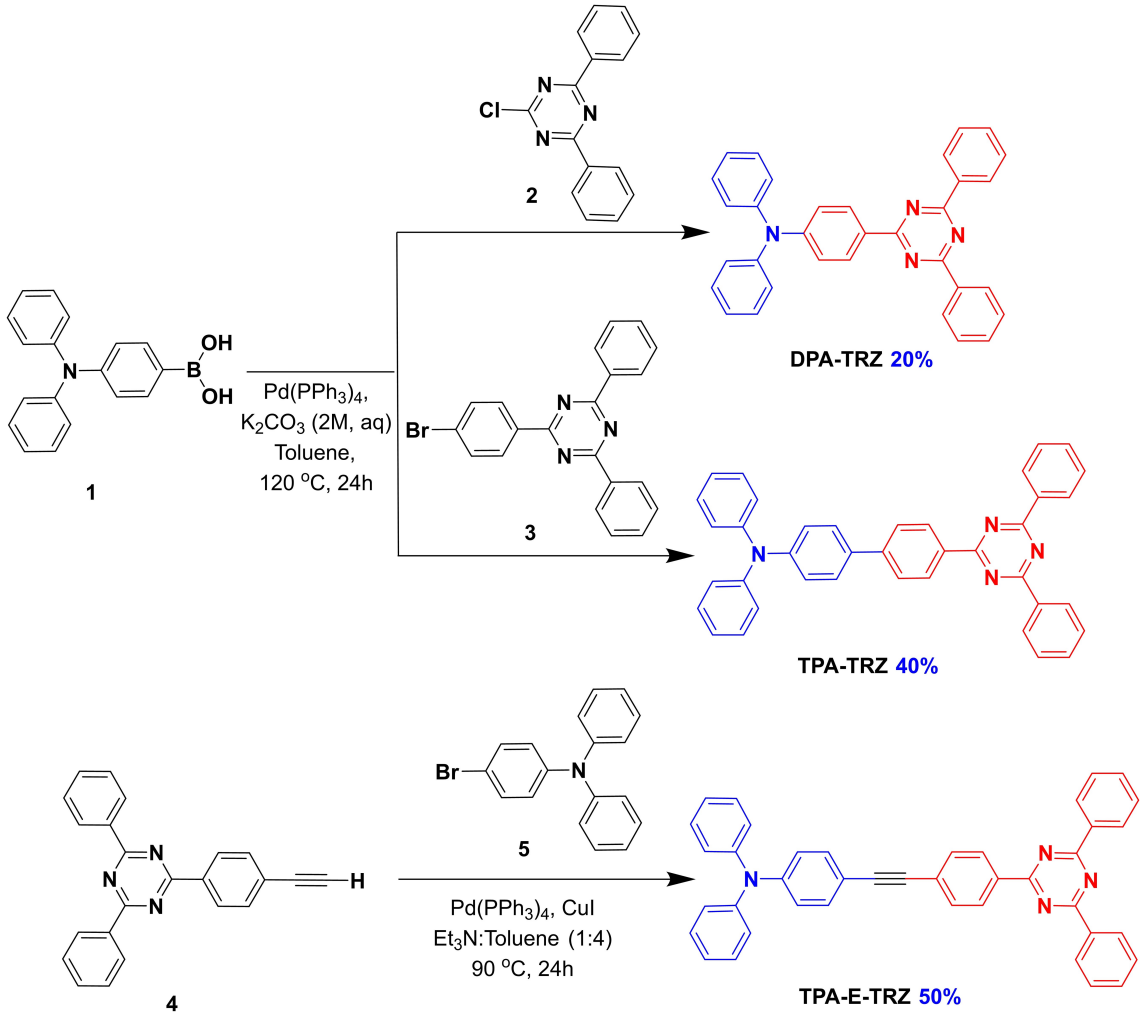

Scheme 1. Synthesis of DPA-TRZ, TPA-TRZ and TPA-E-TRZ.

Single crystal X-ray diffraction analysis

Single crystals of **DPA-TRZ** and **TPA-E-TRZ** were grown by the vapour diffusion of *n*-hexane into a dichloromethane solution of the compound. The molecular structures were determined by single-crystal X-ray diffraction analysis and are shown in Figure 3. As expected, the triphenyl-1,3,5-triazine unit is planar in both **DPA-TRZ** and **TPA-E-TRZ** (root-mean-squared deviation from planarity 0.106 and 0.135 Å, respectively), in agreement with the previously reported single crystal structures of **bis-PXZ-TRZ** and **TRZ-DI**.[17–18] This planarity gives rise to intramolecular C–H···N hydrogen bonds in both compounds, between the triazine nitrogen atoms and the proximal C–H hydrogen atoms on the phenyl rings. Due to the extended nature of **TPA-E-TRZ**, it adopts a subtle curve along the length of the bridge from the TRZ to the amine donor (Figure S**16**). The dihedral angle between the phenoxazine donor and the TRZ acceptor in **bis-PXZ-TRZ** is 88° while the same angle between diindolocarbazole donor and the TRZ acceptor in **TRZ-DI** is 66.9°. In the case of both **DPA-TRZ** and **TPA-E-TRZ**, the torsion angles between the amine donor and the adjacent phenyl of the bridge were much smaller, 39.30(19)° and 32.03(18), respectively (Figure S**17**). The situation in **TPA-E-TRZ** is complicated by the bridging phenyl of the TPA group not being co-planar with the triphenyl-1,3,5-triazine group (angle between planes of the two bridging phenyl groups: 18.19°). This, combined with the torsion angle existing between the amine donor and adjacent phenyl, results in the TPA being nearly co-planar with the triphenyl-1,3,5-triazine (angle between average planes of the TPA and the triphenyl-1,3,5-triazine: 9.40°, Figure S**17**). Much of the inter-planar angle in this case arise from the curve along the length of the **TPA-E-TRZ** molecule.

The solid state packing of each of these compounds is stabilized by intermolecular π-π interactions in both cases, supported by C–H···π interactions in the structure of **TPA-E-TRZ**. The π-π interactions occur between triazine rings and adjacent phenyl rings in **DPA-TRZ**, and between adjacent triazine rings in **TPA-E-TRZ**, at centroid-centroid distances of 3.6409(9) and 3.5260(7) Å, respectively. In **DPA-TRZ** this gives rise to π-stacked chains of molecules running along the crystallographic *b*-axis (Figure S**16**). In contrast, the π-stacking interactions in **TPA-E-TRZ** result in the formation of head-to-head dimers. These dimers are then augmented by the addition of C–H···π interactions between the π-systems of phenyl rings bound to the triazine ring and phenyl–H groups of the TPA subunit of further adjacent molecules, resulting in four-layered sets of interacting molecules. Both outer ends of this tetrameric unit are able to form their own set of four-layered interactions, leading to the formation of one-dimensional zigzag chains propagating along the crystallographic *abc*-diagonal axis (Figure S**16**).

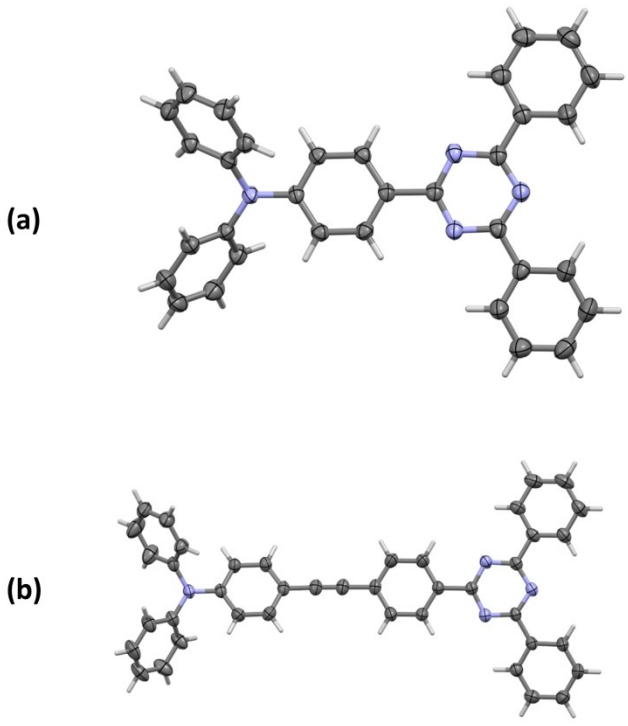

Figure 3. Thermal-ellipsoid plots (ellipsoids drawn at the 50% probability level) of (a) **DPA-TRZ**, and (b) **TPA-E-TRZ**.

Theoretical calculations

Density functional theory (DFT) calculations at the PBE0/6-31G (d,p)[15,19] level of theory were performed to provide insight into the electronic structure of the emitters. The ground state geometries of the molecules were optimized in the gas phase; the starting geometries for **DPA-TRZ** and **TPA-E-TRZ** were obtained from the single crystal X-ray diffraction analysis. Time-dependent DFT calculations were performed within the Tamm–Dancoff approximation (TDA)[20] using the ground state optimized geometries. The energies and electron density distributions of the highest occupied and lowest unoccupied molecular orbitals (HOMO/LUMO) and the energies of the S_1 and T_1 states are shown in Figure 4 and the data is summarized in Table 1. In all three emitters, the HOMO is localized on the triphenylamine donor and the bridging spacer while the LUMO is delocalized over the TRZ acceptor and extending to the diphenylamine donor moiety. A large electron density overlap therefore exists, which is reflected in the large calculated ΔE_{ST} values. Indeed, the calculated ΔE_{ST} for these three emitters are larger than that of structurally similar fluorescent emitter, **CzPhTRZ** and so would be expected to be fluorescent in nature. The HOMO levels for **TPA-TRZ** and **TPA-E-TRZ**, both at −5.22 eV, are destabilized compared to that of **DPA-TRZ** at −5.37 eV, reflecting a similarly large π-conjugation length in these two molecules. The LUMO level becomes progressively more stabilized from **DPA-TRZ** (−1.59 eV) to **TPA-TRZ** (−1.76 eV) to **TPA-E-TRZ** (−1.93 eV) due to an increased delocalization of the π-election density across the series. As a result, the HOMO-LUMO gap decreases across the series from **DPA-TRZ** (ΔE = 3.78 eV) to **TPA-E-TRZ** (ΔE = 3.29 eV). The energy of the emissive S_1 state gradually decreases from 3.25 eV for **DPA-TRZ** to 3.05 eV for **TPA-TRZ** and then to 2.92 eV for **TPA-E-TRZ**. The energy of the T_1 state for both **DPA-TRZ** and **TPA-TRZ** was

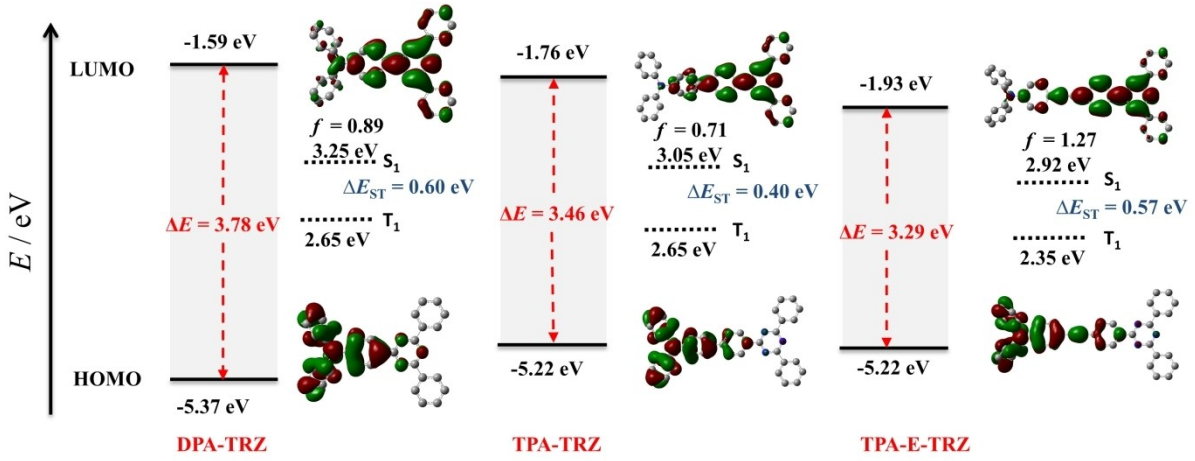

Figure 4. DFT-calculated ground state (PBE0/6-31g(d,p)) and TDA calculated excited state energies and electron density distributions (ISO value = 0.02) of the frontier molecular orbitals of **DPA-TRZ, TPA-TRZ** and **TPA-E-TRZ**.

Table 1. Summary of electrochemical and DFT/TDA calculated photophysical properties.

Emitters	Experimental[a] E^{ox}/E^{red} [V]	HOMO[b]/LUMO[b] [eV]	ΔE[c] [eV]	Calculated HOMO[d]/LUMO[d] [eV]	ΔE[c] [eV]	S_1[d] [eV]	T_1[d] [eV]	ΔE_{ST}[d] [eV]
DPA-TRZ	1.20/−1.67	−5.54/−2.67	2.87	−5.37/−1.59	3.78	3.25	2.65	0.60
TPA-TRZ	1.08/−1.59	−5.42/−2.75	2.67	−5.22/−1.76	3.46	3.05	2.65	0.40
TPA-E-TRZ	1.10/−1.50	−5.44/−2.84	2.60	−5.22/−1.93	3.29	2.92	2.35	0.57

[a] Electrochemical data reported versus SCE in CH_2Cl_2 with 0.1 M $[nBu_4N]PF_6$ as the supporting electrolyte, Pt as the working electrode, Ag/AgCl as the reference electrode and Pt wire as the counter electrode. Fc/Fc^+ was used as the internal reference (0.46 V vs SCE).[22] [b] The HOMO and LUMO energies were calculated using the relation $E_{HOMO}/_{LUMO} = -(E^{ox}/E^{red} + 4.80)$ eV, where E^{ox} and E^{red} are anodic and cathodic peak potentials, respectively, obtained from DPV.[23] [c] $\Delta E = |E_{HOMO} - E_{LUMO}|$. [d] Determined from the DFT or TDA/DFT calculations at PBE0/6-31G(d,p).

predicted to be 2.65 eV while the energy of the same state decreased to 2.35 eV for **TPA-E-TRZ**. The resulting ΔE_{ST} values were found to be 0.60 eV, 0.40 eV and 0.57 eV for **DPA-TRZ**, **TPA-TRZ** and **TPA-E-TRZ**, respectively. The predicted values of S_1 and ΔE_{ST} for **DPA-TRZ** align with those predicted for **CzPhTRZ** ($S_1 = 3.27$ eV, $T_1 = 2.89$ eV and $\Delta E_{ST} = 0.38$) while the T_1 state is significantly more stabilized at the same level of theory.[21]

Electrochemical properties

The electrochemical properties of the three emitters were investigated by cyclic voltammetry (CV) and differential pulse voltammetry (DPV), Figure 5, and the results are compiled in Table 1. The reduction wave is reversible for **DPA-TRZ** and irreversible for **TPA-TRZ** and **TPA-E-TRZ**. The reduction is assigned to the electron-accepting triazine and extends onto the bridging moiety. With increasing conjugation within the bridge there is an expected progressive anodic shift in the reduction potential from −1.67 V to −1.59 V and −1.50 V for **DPA-TRZ** and **TPA-TRZ** and **TPA-E-TRZ**, respectively. The oxidation wave is assigned to the electron-donating triphenylamine unit and found to be reversible for **TPA-TRZ** and quasi-reversible for **DPA-TRZ** and **TPA-E-TRZ**. The oxidation potential shifts cathodically from 1.20 V for **DPA-TRZ** to 1.08 V for **TPA-TRZ**; E_{ox} is not further cathodically shifted for **TPA-E-TRZ** and is found to be 1.10 V. Indeed, DFT calculations predict similar HOMO levels for both **TPA-TRZ** and **TPA-E-TRZ**, both destabilized compared to the HOMO of **DPA-TRZ**. Thus, the electrochemical gap decreases with increasing conjugation with the bridge.

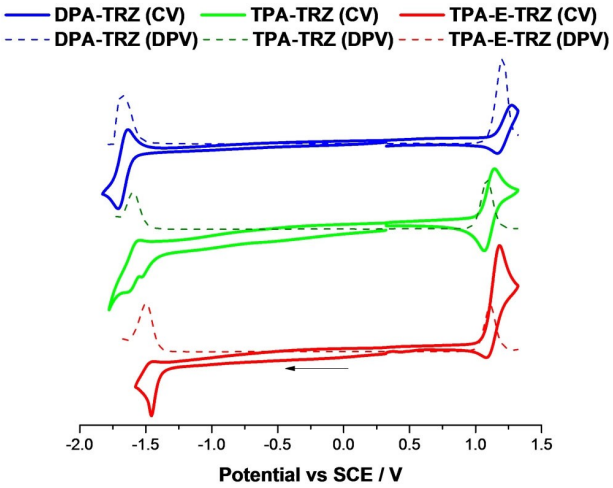

Figure 5. Cyclic voltammograms and DPV scans of emitters (redox scans were carried out in degassed DCM at a scan rate 100 mV s^{-1})

Photophysical properties

The absorption spectra in acetonitrile are shown in Figure 6. In solution, all three emitters exhibit similar absorption profiles with two strong absorption bands around 265 nm and 390 nm. The former is assigned to a locally excited (LE) transition on the amine donor that is progressively red-shifted and become more absorptive with increasing conjugation on the bridge (Tables S1 and S2). The low-energy band is assigned to a charge transfer (CT) transition from the amine donor to the TRZ acceptor. The position of this band is not very sensitive to the nature of the bridge. Interestingly, the trend here in both increasing energy and decreasing molar absorptivity, ε, progresses from **TPA-TRZ** to **DPA-TRZ** to **TPA-E-TRZ**. This suggests that there is more efficient electronic communication in **TPA-TRZ** than in the other two compounds. TD-DFT calculations corroborate the observed trend in S_1 energies and predict that the nature of the S_1 state is a CT transition from donor (TPA) to acceptor (TRZ) in all three emitters. However the oscillator strength (f) for the S_1 state was calculated to be 0.89, 0.71 and 1.27 for **DPA-TRZ**, **TPA-TRZ** and **TPA-E-TRZ**, respectively. Thus, the calculations overemphasize the probability of the HOMO-LUMO transition for **TPA-E-TRZ**.

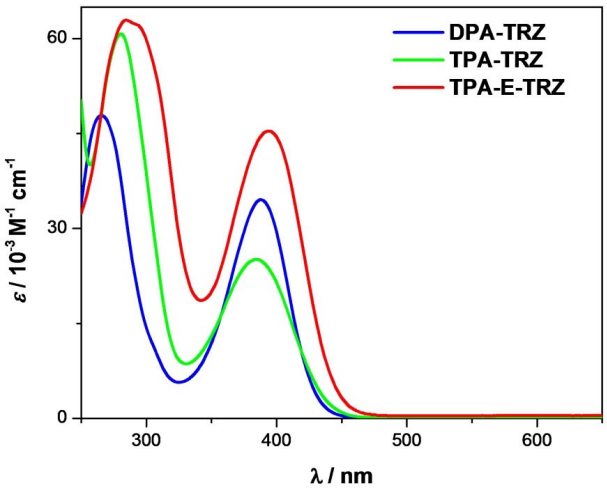

Figure 6. UV-Vis absorption spectra of **DPA-TRZ**, **TPA-TRZ** and **TPA-E-TRZ** in acetonitrile (conc. = 1×10^{-5} M).

The photoluminescence (PL) spectra of the emitters in both DCM and toluene are broad and unstructured, an indication of emission from a CT state (Figure 7). In DCM, **DPA-TRZ** shows blue-green emission with λ_{PL} at 508 nm. The emission is red-shifted to 544 nm for **TPA-TRZ** and 561 nm for **TPA-E-TRZ**. The change in trend for what is observed in the absorption spectra for the CT band suggests that there is a planarization of the conformation of **TPA-TRZ** in the excited state that results in the observed red-shift compared to **DPA-TRZ**. In the less polar solvent toluene, the PL spectra of the three emitters are blue-shifted compared to those in DCM and the magnitude of the red-shift in the emission across the family of emitters is significantly attenuated with λ_{PL} ranging from 456 nm for **DPA-TRZ** to 463 nm for **TPA-TRZ** (Figure 7b). Recorded excitation spectra are in good agreement with absorption spectra in both solvents. The ΔE_{ST} values of 0.26, 0.37, and 0.27 eV were determined from the energy difference between the onset of the prompt fluorescence and phosphorescence spectra in toluene glass at 77 K for **DPA-TRZ, TPA-TRZ** and **TPA-E-TRZ**, respectively (Figure 8). The ΔE_{ST} values for **DPA-TRZ** and **TPA-E-TRZ** are sufficiently small that these two compounds could be TADF compounds, and therefore show promise as emitters in OLEDs. The theoretically calculated energies of the S_1 states for **DPA-TRZ** (3.25 eV), **TPA-TRZ** (3.05 eV) and **TPA-E-TRZ** (2.92 eV)

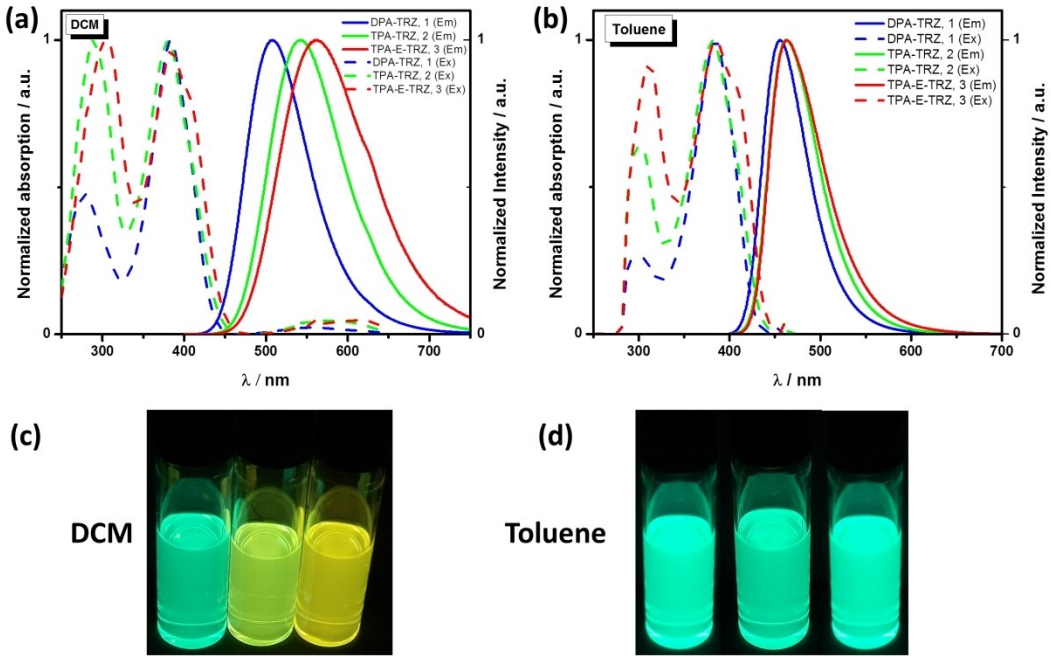

Figure 7. Excitation and PL spectra of the emitters in (a) DCM and (b) toluene (λ_{exc} = 390 nm); (c) and (d) their photographs under UV light (λ_{exc} = 365 nm).

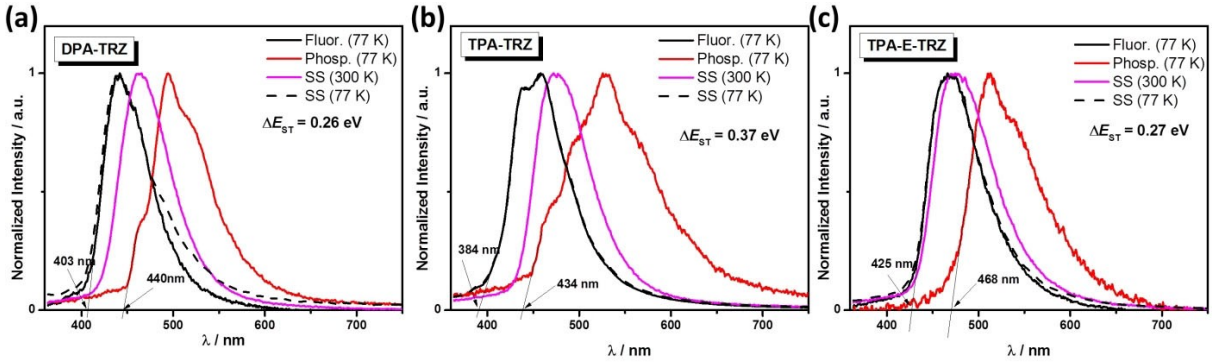

Figure 8. PL spectra of (a) **DPA-TRZ**, (b) TPA-**TRZ** and (c) **TPA-E-TRZ** in toluene, including steady-state (300 K and 77 K), prompt fluorescence (77 K, delay time = 1 ns, time window = 100 ns), and phosphorescence (77 K, delay time = 1 ms, time window = 10 ms) spectra. λ_{exc} = 360 nm.

are in reasonably good agreement with the experimentally determined values of 3.07 eV, 3.22 eV and 2.91 eV, respectively, in toluene glass. On the other hand, the theoretically calculated energies of the T_1 state for **DPA-TRZ**, **TPA-TRZ** and **TPA-E-TRZ** (2.65 eV, 2.65 eV and 2.35 eV) are consistently over-stabilized when compared to their respective measured values of 2.81 eV, 2.85 eV and 2.64 eV, in toluene glass.

All three compounds showed positive solvatochromism with the PL spectra becoming progressively broader with increasing solvent polarity (Figure 9). For both **TPA-TRZ** and **TPA-E-TRZ** the emission spectra in methylcyclohexane become structured and are located at the same energy, indicating an emission from a TPA-based locally-excited (LE) state, while the emission of **DPA-TRZ** remains unstructured and thus even in this non-polar solvent the emission originates from a predominantly CT state.

We next explored the photophysical properties of the three emitters in the solid state, the data of which is summarized in Table 2. The PL spectra of **DPA-TRZ, TPA-TRZ** and **TPA-E-TRZ** in 10 wt% doped PMMA films and neat films are shown in Figure 10. The trend observed in solution is reproduced in both 10 wt% PMMA and neat films. The emission spectra in the neat films are red-shifted compared to the 10 wt% PMMA films, likely a result of a combination of increased polarity of the medium and enhanced exciplex emission at elevated concentration.[24] The photoluminescence quantum yields, Φ_{PL}, in 10 wt% PMMA films are high at 73%, 67% and 67% for **DPA-TRZ, TPA-TRZ** and **TPA-E-TRZ**, respectively. The Φ_{PL} values are somewhat decreased in the neat film at 55%, 53% and 49%, respectively. Among these three emitters, **DPA-TRZ** shows biexponential emission decay kinetics while **TPA-TRZ** and **TPA-E-TRZ** display triexponential decay in both PMMA host and neat film (Figure 11). Both **TPA-TRZ** and **TPA-E-TRZ** undergo slower PL decay in both PMMA and in neat film compared to **DPA-TRZ**, reflecting perhaps the larger conformational changes that occur

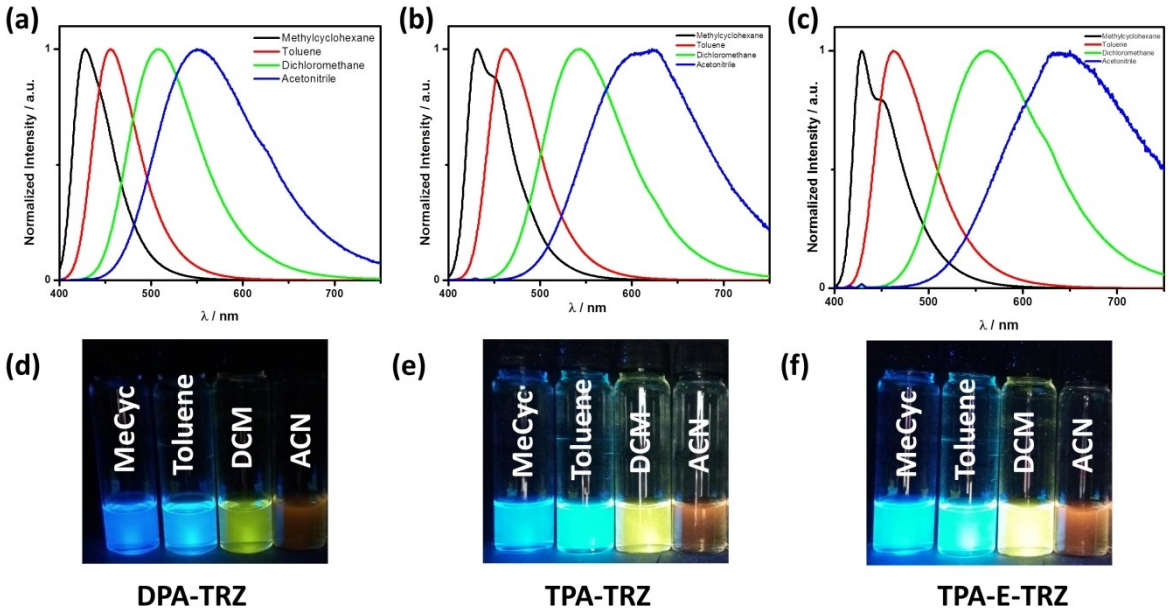

Figure 9. Solvatochromic PL spectra of (a) **DPA-TRZ**, (b) **TPA-TRZ**, and (c) **TPA-E-TRZ** (λ_{exc} = 390 nm). Photograph of (d) **DPA-TRZ**, (e) **TPA-TRZ**, and (f) **TPA-E-TRZ** under UV light. (λ_{exc} = 365 nm). Note that photos were taken with two different cameras and cross-comparison between the photos is not advisable.

Table 2. Summary of the photophysical properties of DPA-TRZ, TPA-TRZ and TPA-E-TRZ.

Emitter	Absorption[a] [nm] (ε /×10^{-3} M^{-1}cm^{-1})	Solution[b] DCM [nm]	Toluene [nm]	10 wt% PMMA film $\lambda^{[c]}$ [nm]; Φ_{PL}[d] [%]; τ_{PL}[e] [ns]	Neat film $\lambda^{[c]}$ [nm]; Φ_{PL}[d][%]; τ_{PL}[e][ns]	ΔE_{ST}[f] [eV]
DPA-TRZ	266(47), 388(34)	508	456	479; 64(73); 3, 6	482; 56(55); 3, 5	0.26
TPA-TRZ	281(60), 385(25)	544	463	483; 65(67); 2, 4, 15	497; 52(53); 2, 6, 18	0.37
TPA–E-TRZ	284(64), 394(45)	561	462	508; 67(67); 2, 4, 18	502; 49(49); 1, 5, 17	0.27

[a] Measured in MeCN at 298 K. [b] λ_{exc} = 390 nm. [c] λ_{exc} = 378 nm. [d] Absolute Φ_{PL} values measured under air with those measured under N_2 given in parentheses. [e] λ_{exc} = 378 nm. [f] Measured as the energy difference between onsets of the prompt fluorescence (at 77 K in toluene, λ_{exc} = 360 nm, time delay = 1 ns, time window: 100 ns) and the phosphorescence (at 77 K in toluene, λ_{exc} = 360 nm, time delay = 1 ms, time window = 10 ms).

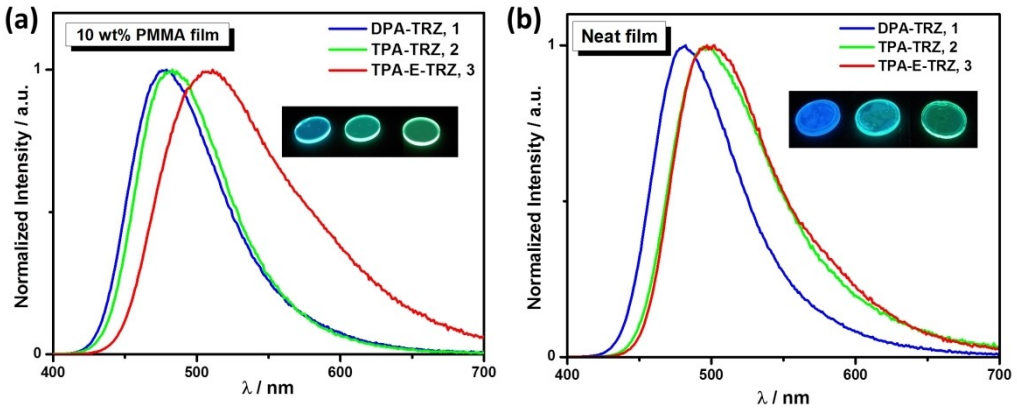

Figure 10. PL spectra of **DPA-TRZ, TPA-TRZ** and **TPA-E-TRZ** in (a) 10 wt% doped PMMA films and (b) neat films. Insets show photos of the films (λ_{exc} = 390 nm for spectra and λ_{exc} = 365 for photos). Note that photos were taken with two different cameras and cross-comparison between the photos is not advisable.

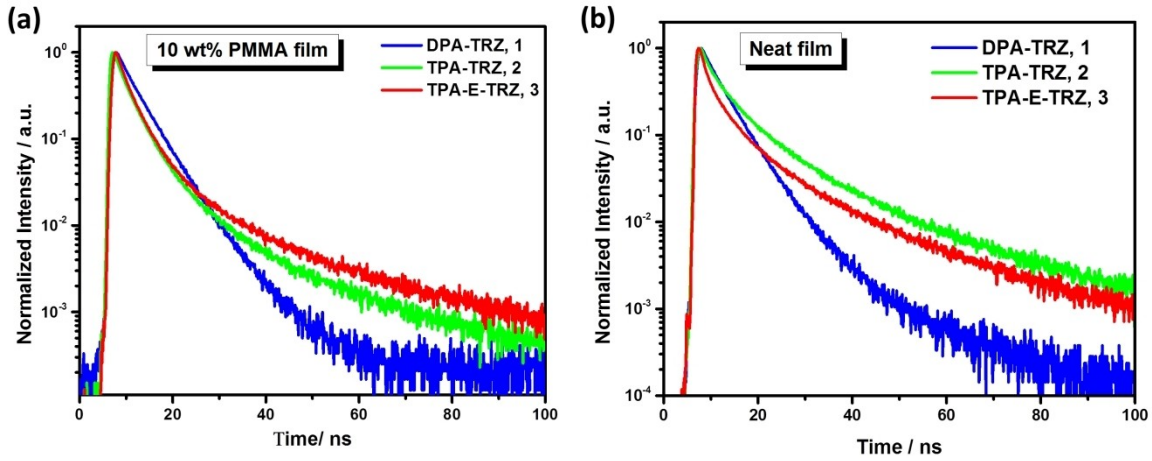

Figure 11. PL decay profiles for **DPA-TRZ, TPA-TRZ** and **TPA-E-TRZ** in (a) 10 wt% PMMA matrix and (b) neat film (λ_{exc} = 378 nm).

in these two compounds in the excited state. A summary of the photophysical properties is given in Table 2.

Conclusion

We reported three structurally related donor-acceptor emitters based on a triazine acceptor and a triaryl amine donor. We showed how the absorption and emission could be progressively red-shifted with increasing conjugation of the bridging moiety. The correlation to the structure was dependent on the distinct conformations in the ground and excited state. Although the experimentally determined ΔE_{ST} of these materials are comparable to those reported for TADF emitters in the literature, we did not observe any TADF character in the time-resolved PL in both doped and neat films.

Supporting information

General experimental procedures, synthesis, melting point, NMR spectra, HRMS spectra, elemental analysis report, HPLC analysis report, crystallographic data (CCDC 1992627-1992628), molecular orbitals and Cartesian coordinates of optimized ground states are provided in supplementary information.

Acknowledgement

SK acknowledges the financial support from European Union's Horizon 2020 research and innovation programme under Marie Skłodowska Curie Individual Fellowship (MCIF; Agreement No. 748430-THF-OLED). We thank the EPSRC UK National Mass Spectrometry Facility at Swansea University for analytical services. We thank UMICORE AG for the gift of catalysts.

Conflict of Interest

The authors declare no conflict of interest.

Keywords: donor-acceptor · charge transfer · fluorescence · thermally activated delayed fluorescence · triazine

[1] Y. Sun, N. C. Giebink, H. Kanno, B. Ma, M. E. Thompson, S. R. Forrest, *Nature* **2006**, *440*, 908–912.
[2] A. Endo, M. Ogasawara, A. Takahashi, D. Yokoyama, Y. Kato, C. Adachi, *Adv. Mater.* **2009**, *21*, 4802–4806.
[3] M. Y. Wong, E. Zysman-Colman, *Adv. Mater.* **2017**, *29*, 1605444.
[4] P. Data, Y. Takeda, *Chem. Asian J.* **2019**, *14*, 1613–1636.
[5] G. Schwartz, S. Reineke, T. C. Rosenow, K. Walzer, K. Leo, *Adv. Funct. Mater.* **2009**, *19*, 1319–1333.
[6] H. Uoyama, K. Goushi, K. Shizu, H. Nomura, C. Adachi, *Nature* **2012**, *492*, 234–238.
[7] P. L. dos Santos, D. Chen, P. Rajamalli, T. Matulaitis, D. B. Cordes, A. M. Z. Slawin, D. Jacquemin, E. Zysman-Colman, I. D. W. Samuel, *ACS Appl. Mater. Interfaces* **2019**, *11*, 45171–45179.
[8] A. Endo, K. Sato, K. Yoshimura, T. Kai, A. Kawada, H. Miyazaki, C. Adachi, *Appl. Phys. Lett.* **2011**, *98*, 083302.
[9] L. S. Cui, H. Nomura, Y. Geng, J. U. Kim, H. Nakanotani, C. Adachi, *Angew. Chem. Int. Ed.* **2017**, *56*, 1571–1575; *Angew. Chem.* **2017**, *129*, 1593–1597.
[10] H. Tanaka, K. Shizu, H. Miyazaki, C. Adachi, *Chem. Commun.* **2012**, *48*, 11392–11394.
[11] H. Tanaka, K. Shizu, H. Nakanotani, C. Adachi, *J. Phys. Chem. C* **2014**, *118*, 15985–15994.
[12] W.-L. Tsai, M.-H. Huang, W.-K. Lee, Y.-J. Hsu, K.-C. Pan, Y.-H. Huang, H.-C. Ting, M. Sarma, Y.-Y. Ho, H.-C. Hu, C.-C. Chen, M.-T. Lee, K.-T. Wong, C.-C. Wu, *Chem. Commun.* **2015**, *51*, 13662–13665.
[13] J. Lee, K. Shizu, H. Tanaka, H. Nakanotani, T. Yasuda, H. Kaji, C. Adachi, *J. Mater. Chem. C* **2015**, *3*, 2175–2181.
[14] K. Shizu, M. Uejima, H. Nomura, T. Sato, K. Tanaka, H. Kaji, C. Adachi, *Phys. Rev. Appl.* **2015**, *3*, 014001.
[15] Y. Geng, A. D'Aleo, K. Inada, L.-S. Cui, J. U. Kim, H. Nakanotani, C. Adachi, *Angew. Chem. Int. Ed.* **2017**, *56*, 16536–16540; *Angew. Chem.* **2017**, *129*, 16763–16767.
[16] R. Furue, T. Nishimoto, I. S. Park, J. Lee, T. Yasuda, *Angew. Chem. Int. Ed.* **2016**, *55*, 7171–7175; *Angew. Chem.* **2016**, *128*, 7287–7291.
[17] H. Tanaka, K. Shizu, H. Nakanotani, C. Adachi, *Chem. Mater.* **2013**, *25*, 3766–3771.
[18] K. J. Kim, G. H. Kim, R. Lampande, D. H. Ahn, J. B. Im, J. S. Moon, J. K. Lee, J. Y. Lee, J. Y. Lee, J. H. Kwon, *J. Mater. Chem. C* **2018**, *6*, 1343–1348.
[19] C. Adamo, V. Barone, *J. Chem. Phys.* **1999**, *110*, 6158–6170.
[20] S. Hirata, M. Head-Gordon, *Chem. Phys. Lett.* **1999**, *314*, 291–299.
[21] N. Sharma, E. Spuling, C. M. Mattern, W. Li, O. Fuhr, Y. Tsuchiya, C. Adachi, S. Bräse, I. D. W. Samuel, E. Zysman-Colman, *Chem. Sci.* **2019**, *10*, 6689–6696.
[22] N. G. Connelly, W. E. Geiger, *Chem. Rev.* **1996**, *96*, 877–910.
[23] C. M. Cardona, W. Li, A. E. Kaifer, D. Stockdale, G. C. Bazan, *Adv. Mater.* **2011**, *23*, 2367–2371.
[24] P. L. dos Santos, F. B. Dias, A. P. Monkman, *J. Phys. Chem. C* **2016**, *120*, 18259–18267.

Manuscript received: March 29, 2020
Revised manuscript received: May 11, 2020
Accepted manuscript online: May 12, 2020
Version of record online: ■■, ■■■

ACES Asian Chemical Editorial Society

ASIAN JOURNAL OF ORGANIC CHEMISTRY Communication

COMMUNICATION

Bridging donors and acceptors: We present a structure-property relationship study whereby we explore the effect of conjugation length of the bridging moiety on the optoelectronic properties were investigated of the compounds in a family of donor-bridge-acceptor emitters. This experimental study is supported by density functional theory calculations.

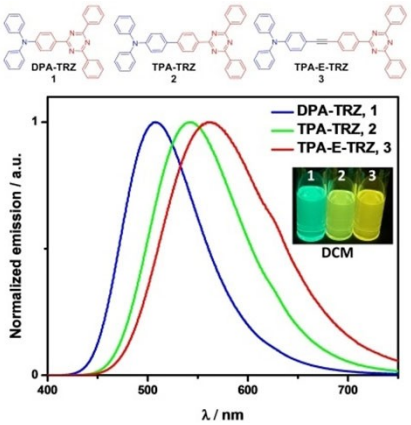

*Dr. S. Kumar, Prof. P. Rajamalli, Dr. D. B. Cordes, Prof. A. M. Z. Slawin, Prof. E. Zysman-Colman**